J|A|C|S
ARTICLES
Published on Web 08/29/2002

The First Example of a Nitrile Hydratase Model Complex that Reversibly Binds Nitriles

Jason Shearer,[†] Henry L. Jackson,[†] Dirk Schweitzer,[†] Durrell K. Rittenberg,[†] Tanya M. Leavy,[‡] Werner Kaminsky,[§] Robert C. Scarrow,*[,‡] and Julie A. Kovacs*[,†]

Contribution from the Department of Chemistry, University of Washington, Box 351700, Seattle, Washington 98195, and The Department of Chemistry, Haverford College, Haverford, Pennsylvania 19041

Received November 16, 2001

Abstract: Nitrile hydratase (NHase) is an iron-containing metalloenzyme that converts nitriles to amides. The mechanism by which this biochemical reaction occurs is unknown. One mechanism that has been proposed involves nucleophilic attack of an Fe-bound nitrile by water (or hydroxide). Reported herein is a five-coordinate model compound ($[Fe^{III}(S_2{}^{Me2}N_3(Et,Pr))]^+$) containing Fe(III) in an environment resembling that of NHase, which reversibly binds a variety of nitriles, alcohols, amines, and thiocyanate. XAS shows that five-coordinate $[Fe^{III}(S_2{}^{Me2}N_3(Et,Pr))]^+$ reacts with both methanol and acetonitrile to afford a six-coordinate solvent-bound complex. Competitive binding studies demonstrate that MeCN preferentially binds over ROH, suggesting that nitriles would be capable of displacing the H_2O coordinated to the iron site of NHase. Thermodynamic parameters were determined for acetonitrile ($\Delta H = -6.2(\pm0.2)$ kcal/mol, $\Delta S = -29.4(\pm0.8)$ eu), benzonitrile ($-4.2(\pm0.6)$ kcal/mol, $\Delta S = -18(\pm3)$ eu), and pyridine ($\Delta H = -8(\pm1)$ kcal/mol, $\Delta S = -41(\pm6)$ eu) binding to $[Fe^{III}(S_2{}^{Me2}N_3(Et,Pr))]^+$ using variable-temperature electronic absorption spectroscopy. Ligand exchange kinetics were examined for acetonitrile, *iso*-propylnitrile, benzonitrile, and 4-*tert*-butylpyridine using ^{13}C NMR line-broadening analysis, at a variety of temperatures. Activation parameters for ligand exchange were determined to be $\Delta H^{\ddagger} = 7.1(\pm0.8)$ kcal/mol, $\Delta S^{\ddagger} = -10(\pm1)$ eu (acetonitrile), $\Delta H^{\ddagger} = 5.4(\pm0.6)$ kcal/mol, $\Delta S^{\ddagger} = -17(\pm2)$ eu (*iso*-propionitrile), $\Delta H^{\ddagger} = 4.9(\pm0.8)$ kcal/mol, $\Delta S^{\ddagger} = -20(\pm3)$ eu (benzonitrile), and $\Delta H^{\ddagger} = 4.7(\pm1.4)$ kcal/mol $\Delta S^{\ddagger} = -18(\pm2)$ eu (4-*tert*-butylpyridine). The thermodynamic parameters for pyridine binding to a related complex, $[Fe^{III}(S_2{}^{Me2}N_3(Pr,Pr))]^+$ ($\Delta H = -5.9(\pm0.8)$ kcal/mol, $\Delta S = -24(\pm3)$ eu), are also reported, as well as kinetic parameters for 4-*tert*-butylpyridine exchange ($\Delta H^{\ddagger} = 3.1(\pm0.8)$ kcal/mol, $\Delta S^{\ddagger} = -25(\pm3)$ eu). These data show for the first time that, when it is contained in a ligand environment similar to that of NHase, Fe(III) is capable of forming a stable complex with nitriles. Also, the rates of ligand exchange demonstrate that low-spin Fe(III) in this ligand environment is more labile than expected. Furthermore, comparison of $[Fe^{III}(S_2{}^{Me2}N_3(Et,Pr))]^+$ and $[Fe^{III}(S_2{}^{Me2}N_3(Pr,Pr))]^+$ demonstrates how minor distortions induced by ligand constraints can dramatically alter the reactivity of a metal complex.

Performing reactions under environmentally friendly conditions has recently become a desirable goal in the search for new catalysts.[1] Enzymes are often viewed as ideal in this respect because of their ability to perform chemical transformations under mild conditions with high yields and stereospecificity.[2] Nitrile hydratase (NHase) is an example of a metalloenzyme that is used industrially, in the multikiloton production of acrylamide from acrylonitrile.[3] NHase is a mononuclear thiolate-ligated non-heme iron (or noncorrinoid cobalt) metalloenzyme, which converts nitriles to amides.[4] Of the two metal-containing forms, Co−NHase and Fe−NHase, the iron form has been the most extensively studied.[5] On the basis of EXAFS, EPR, and two X-ray crystal structures, Fe−NHase has been shown to

* To whom correspondence should be addressed. E-mail: kovacs@chem.washington.edu.
[†] University of Washington.
[‡] Haverford College.
[§] Staff crystallographer.

(1) Clark, J. H. *Pure Appl. Chem.* **2001**, *73*, 103−111.
(2) Faber, K.; Patel, R. *Curr. Opin. Biotechnol.* **2000**, *11*, 517−519.
(3) Kobyashi, M.; Nagasawa, T.; Yamada, H. *Tibtech* **1992**, *10*, 402−408.
(4) (a) Kobyashi, M. *Nat. Biotechnol.* **1998**, *16*, 733−736. (b) Shearer, J.; Kovacs, J. A. Nitrile hydratase: An unusual Fe(III) ligated metalloenzyme. *Encyclopedia of Catalysis*; John Wiley & Sons: New York, 2002, in press.
(5) (a) Huang, W.; Jia, J.; Cummings, J.; Nelson, M.; Schneider, G.; Lindqvist, Y. *Structure* **1997**, *5*, 691−699. (b) Nagashima, S. N.; Naoshi, D.; Tsujimura, M.; Takio, K.; Odaka, M.; Yohda, M.; Kamiya, N.; Endo, I. *Nat. Struct. Biol.* **1998**, *5*, 347−351. (c) Nelson, M. J.; Jin, H.; Turner, M. I., Jr.; Grove, G.; Scarrow, R. C.; Brennan, B. A.; Que, L., Jr. *J. Am. Chem. Soc.* **1991**, *113*, 7072−7073. (d) Nagamune, T.; Honda, J.; Kobayashi, Y.; Sasabe, H.; Endo, I.; Ambe, F. *Hyperfine Interact.* **1992**, *71*, 1271−1274. (e) Brennan, B. A.; Cummings, J. G.; Chase, D. B.; Turner, M. I., Jr.; Nelson, M. J. *Biochemistry* **1996**, *35*, 10068−10077 (the pH = 9.0 form of NHase has been shown to be inactive). (f) Jin, H.; Turner, I. M.; Nelson, M. J.; Gurbiel, R. J.; Doan, P. E.; Hoffman, B. M. *J. Am. Chem. Soc.* **1993**, *115*, 5290−5291. (g) Payne, M. S.; Wu, S.; Fallon, R. D.; Tudor, G.; Stieglitz, B.; Turner, I. M., Jr.; Nelson, M. J. *Biochemistry* **1997**, *36*, 5447−5454. (h) Nojiri, M.; Nakayama, H.; Odaka, M.; Yohda, M.; Takio, K.; Endo, I. *FEBS Lett.* **2000**, *465*, 173−177. (i) Odaka, M.; Fujii, K.; Hoshino, M.; Noguchi, T.; Tsujimura, M.; Nagashima, S.; Yohda, M.; Nagamune, T.; Inoue, Y.; Endo, I. *J. Am. Chem. Soc.* **1997**, *119*, 3785−3791. (j) Popescu, V.-C.; Münck, E.; Fox, B. G.; Sanakis, Y.; Cummings, J. G.; Turner, I. M., Jr.; Nelson, M. J. *Biochemistry*, **2001**, *40*, 7984−7991.

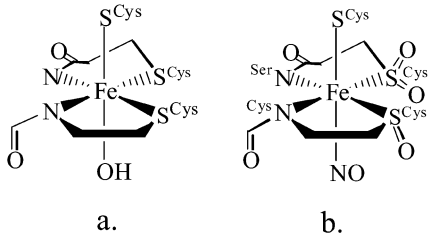

Figure 1. (a) Active-site of NHase as determined by X-ray crystallography (2.65 Å resolution). (b) Active site of NO-inactivated NHase as determined by X-ray crystallography (1.7 Å resolution).

Scheme 1. Three Proposed Mechanisms for Nitrile Hydration by NHase: (1) Involving the Metal Site Serving as a Basic Hydroxide Source, (2) Involving the Metal Site Serving as a Nucleophilic Hydroxide Source, or (3) Involving the Metal Ion Acting as a Lewis Acid and Activating a Metal-Coordinated Nitrile

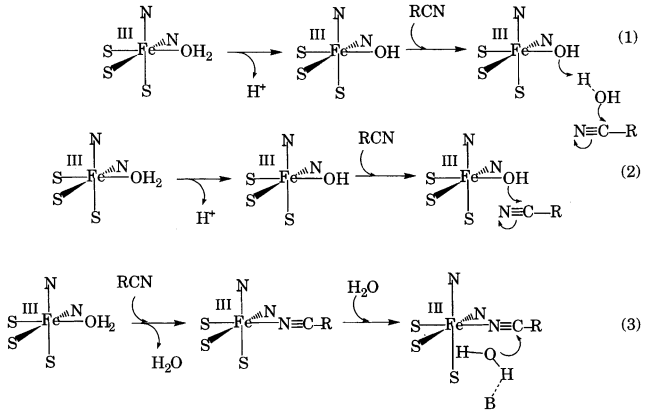

contain a non redox-active Fe(III) ion ligated by two nitrogen donors (derived from amides in the peptide backbone), three cysteinate donors, and either a water or hydroxide (active form), or an NO (inactive form), in a site trans to a cysteinate (Figure 1). The higher-resolution crystal structure[5b] of NO-inhibited Fe−NHase revealed that two of the three cysteinates were oxygenated to either a sulfinate or a sulfenate. It has yet to be proven definitively whether both of these oxidized cysteinates are required for activity.

Although the active-site structure of NHase has been defined, a number of unanswered questions have yet to be adequately addressed. Most importantly, the mechanism of nitrile hydrolysis has yet to be determined. Three distinct mechanisms have been proposed (Scheme 1).[5a] Two of these (mechanisms 1 and 2) involve the metal ion serving as a hydroxide source for the nucleophilic attack at an uncoordinated nitrile, with (mechanism 1), or without (mechanism 2) the involvement of an intervening water molecule. The third (mechanism 3) involves the metal ion acting as a Lewis acid in the activation of a coordinated nitrile for nucleophilic attack by an uncoordinated water. The last two mechanisms are differentiated from the first, in that they involve metal-bound intermediates, and require that the metal ion release product at reasonably fast rates. One might predict that this would be problematic for "substitution inert" low-spin Co(III) and low-spin Fe(III). We've shown, however, that *trans*-thiolates enhance ligand dissociation rates significantly, making low-spin Co(III) and Fe(III) reasonably labile.[13,41] There is spectroscopic evidence that supports mechanism 3.[6] Both the EPR signal and electronic absorption spectrum change

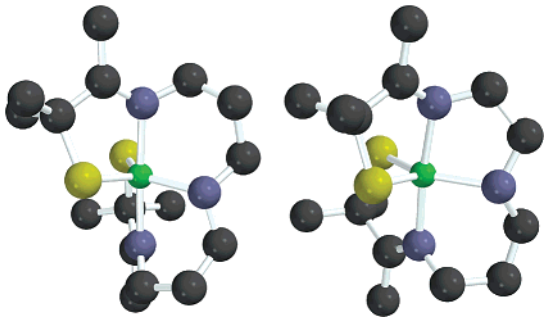

Figure 2. Spartan figure comparing the structures of $[Fe(III)(S_2^{Me2}N_3(Pr,Pr))]^+$ (**1**) and $[Fe(III)(S_2^{Me2}N_3(Et,Pr))]^+$ (**2**).

upon the introduction of nitriles to NHase.[6] One could interpret this to mean that nitriles coordinate to the metal ion; however, it is also possible that the nitrile indirectly perturbs the metal ion by slightly distorting its structure when it "wedges" itself in the active-site pocket. There is also literature precedent for mechanism 3.[7,8] Ford and co-workers have shown[8] that by coordinating nitriles to a metal ion, nitrile hydrolysis rates are enhanced by as much as 10^6 relative to that in the absence of the metal ion. Metal ions in the +3 oxidation state were shown to enhance rates more than those in the +2 oxidation state, suggesting that the metal ion activates the nitrile by acting as a Lewis acid (ie, via an inductive effect), as opposed to via π-back-donation into the nitrile π^* orbitals. Recently Mascharak and co-workers described[9] a five-coordinate Fe(III)−NHase model complex which binds hydroxide, water, and pyridine; this complex would not bind nitriles. On the basis of these results, Mascharak proposed that mechanism 2 was more likely to be operative in NHase than the other two.

We previously reported a five-coordinate coordinatively unsaturated NHase model compound $[Fe(III)(S_2^{Me2}N_3(Pr,Pr))]^+$ (**1**) containing Fe(III) ligated by *cis*-thiolates and imine nitrogens (Figure 2).[10] Munck and Nelson recently proposed, on the basis of low-temperature Mossbauer and EPR experiments, that a five-coordinate NHase intermediate is formed via the flash photolysis of NO from the NO-inactivated form of Fe−NHase.[11] The parameters of these spectra compare well with those of **1**.[12] Compound **1** was shown to bind azide[10a] (a NHase inhibitor) and NO[10b] (a NHase inactivator) trans to a thiolate. The azide-bound complex reproduces the key magnetic and spectroscopic features of NHase including spin state ($S = {}^1/_2$), EPR, low-energy LMCT band in the electronic absorption spectrum ($\lambda_{max} \approx 700$ nm), and average metal−ligand bond lengths.[10a] However, it appeared that **1** would not bind either the substrate or product of NHase. To increase the reactivity of $[Fe(III)(S_2^{Me2}N_3(Pr,Pr))]^+$ (**1**), and yet preserve the coordination environment about the metal center, one methylene group was removed from the ligand backbone to afford $[Fe(III)(S_2^{Me2}N_3(Et,Pr))](PF_6)$ (**2**).[13] This caused the structure to distort, from approximately

(6) Sugiura, Y.; Kuwahara, J.; Nagasawa, T.; Yamada, H. *J. Am. Chem. Soc.* **1987**, *109*, 5848−5850.
(7) Kim, J. H.; Britten, J.; Chin, J. *J. Am. Chem. Soc.* **1993**, *115*, 3618−3622.
(8) Zanella, A. W.; Ford, P. C. *Inorg. Chem.* **1975**, *14*, 42−47.
(9) Noveron, J. C.; Olmstead, M. M.; Mascharak, P. K. *J. Am. Chem. Soc.* **2001**, *123*, 3247−3249.
(10) (a) Ellison, J. J.; Niestedt, A.; Shoner, S. C.; Barnhart, D.; Cowen, J. A.; Kovacs, J. A. *J. Am. Chem. Soc.* **1998**, *120*, 5691−5700. (b) Schweitzer, D.; Ellison, J. J.; Shoner, S. C.; Lovell, S.; Kovacs, J. A *J. Am. Chem. Soc.* **1998**, *120*, 10996−10997.
(11) Popescu, V.-C.; Munck, E.; Fox, B. G.; Sanakis, Y.; Cummings, J.; Turner, I. M., Jr.; Nelson, M. J. *Biochemistry* **2001**, *40*, 7984−7991.
(12) Krebs, C.; Pereira, A. S.; Tavares, P.; Huynh, B. H.; Schweitzer, D.; Ellison, J. J.; Kovacs, J. A. Manuscript in preparation.

trigonal bipyramidal toward a more square pyrimidal structure, and increased the complex's reactivity toward a number of ligands. For example, (Et,Pr)-ligated **2** was shown to have an ~10-fold greater affinity for azide relative to **1**.[13] Complex **2** was also found to bind a variety of other ligands, including nitriles. Herein, we describe the reactivity of **2** with a variety of ligands, and examine the kinetics and thermodynamics of nitrile binding.

Experimental Section

General Synthetic Methods. All manipulations were performed under an atmosphere of dinitrogen using either glovebox or standard Schlenk techniques. Chemical reagents purchased from commercial vendors were of the highest purity available and used without further purification. Solvents were dried using standard procedures and rigorously degassed prior to use. Labeled $Me^{13}CN$ and CD_2Cl_2 were both obtained from Cambridge Isotope Labs (Andover, MA). $[Fe(III)(S_2^{Me2}N_3(Pr,Pr))]^+$ (**1**), $[Fe(III)(S_2^{Me2}N_3(Et,Pr))]^+$ (**2**), and $[Fe(III)(S^{Me2}N_5(tren)(MeCN))]^{2+}$ (**3**) were all prepared as previously described.[10,13−14] Elemental analyses were performed by Atlantic Microlabs (Norcross, GA).

General Instrumental Methods. Solution-state magnetic moments were determined using the Evans' method as modified for superconducting solenoids, on a Bruker AF300 FTNMR spectrometer.[15] EPR spectra were recorded on an X-band Bruker EPX CW EPR spectrometer at 130 K in a CH_2Cl_2/toluene glass, unless otherwise stated. XAS data refinements were performed using *Igor Pro 3.15*.[16] NMR spectra were recorded on a Bruker DPX 500 and DRX 750 FTNMR and are referenced to an external standard of TMS. The temperature of the spectrometer was determined using Van Geet's method.[17] Peaks were fit to a Lorenzian curve using the NMR data analysis package *NUTS*.[18] Electronic absorption spectra were recorded on a Hewlett-Packard 8452A diode array spectrophotometer. Variable-temperature electronic absorption spectra were recorded in a custom-built low-temperature copper-block fitted with a heater, controlled via a thermocouple, and inserted into a stainless steel cryostat.

Preparation of $[Fe(III)(S_2^{Me2}N_3(Et,Pr))(NCS)]$ (2-NCS). Tetrakismethylammonium thiocyanate (410 mg, 3.10 mmol) was added to a MeCN solution (25 mL) of **2** (800 mg, 1.55 mmol), and the solution was stirred for 0.5 h. Diethyl ether (25 mL) was added to precipitate out less soluble impurities. The solids were filtered through a bed of Celite and the volatiles evaporated to dryness under reduced pressure. The resulting red residue was extracted with THF, filtered, and evaporated to dryness, affording 300 mg of **2-NCS** as a red powder (45% yield). Electronic absorption spectrum (CH_2Cl_2): λ_{max} (ϵ_M) 478 (1350), 833 (1020). EPR: $g = 2.183, 2.164, 2.004$. IR (KBr pellet) ν (cm^{-1}): 2058 (thiocyanate). Anal. Calcd for $FeC_{16}H_{29}N_4S_3$: C, 44.75; H, 6.81; N, 13.05. Found: C, 45.28; H, 6.93; N, 12.67.

Ligand Binding Studies. The reactivity of **1** and **2** with neutral and anionic ligands was screened by X-band EPR at 150 K. All EPR spectra were recorded in a toluene/methylene chloride glass (1:1) using a 1000-fold excess of ligand relative to metal complex. Ligand binding causes the distorted pseudorhombic EPR signal associated with **1** and **2** to become more rhombic and the *g*-spread to increase. Once ligands were identified which bind to these metal centers at 150 K, they were then screened for reactivity at higher temperatures (between −90 °C and ambient temperature) using variable-temperature electronic absorption spectroscopy. Ligand binding to **1** and **2** causes a low-energy LMCT band centered near 800 nm to grow in. In this manner, the reactivity of **1** and **2** with a variety of ligands was examined.

Thermodynamics of Nitrile and Pyridine Binding. Equilibrium constants for neutral ligands binding to **1** and **2** were determined in the manner previously described for anionic ligands.[10a] Methylene chloride solutions of **1** and **2** were prepared and then diluted with a methylene chloride solution containing the ligand (acetonitrile, benzonitrile, *iso*-propionitrile, or pyridine), so as to afford a final concentration of ligand-bound complex of 0.300 mM. Ligand concentrations were selected so that between 20 and 80% of the ligand-bound complex would result. Extinction coefficients for the nitrile complexes $[Fe(III)(S_2^{Me2}N_3(Et,Pr))(NCR)]^+$ (**2-NCR**) were determined at −90 °C using a 4000-fold excess of nitrile, and were found to vary insignificantly with varying R groups. All binding measurements for **2-NCMe** and **2-NCPh** were performed at 546, and 839 nm, respectively—the wavelengths which gave the most consistent results. Extinction coefficients for $[Fe(III)(S_2^{Me2}N_3(Pr,Pr))(py)]^+$ (**1-py**) and $[Fe(III)(S_2^{Me2}N_3(Et,Pr))(py)]^+$ (**2-py**) were determined at −90 °C using a 4000-fold excess of pyridine. Equilibrium constants were measured at 656 nm for **1-py** and at 554 nm for **2-py**, over the temperature range −40° to −90 °C. Thermodynamic parameters were then obtained from van't Hoff plots.

NMR Exchange Kinetics. Kinetic parameters for nitrile exchange from **2** were measured using NMR line-width analysis over the temperature range of 190−300 K in CD_2Cl_2. The line-width of the α carbon on the nitrile, with and without the metal complex, ($\Delta\nu_{cplx}$ and $\Delta\nu_{solv}$), are related to the total transverse (spin−spin) relaxation rate, T_{2P}^{-1}, by eq 1:

$$(T_{2P}P_M)^{-1} = \pi(\Delta\nu_{cplx} - \Delta\nu_{solv})P_M^{-1} \quad (1)$$

where P_M is the partial molar fraction of nitrile bound to the metal complex. $(T_{2P}P_M)^{-1}$ can also be expressed as:

$$(T_{2P}P_M)^{-1} = \tau_m^{-1}\frac{T_{2M}^{-2} + (T_{2M}\tau_m)^{-1} + \Delta\omega_M^2}{(T_{2M}^{-1} + \tau_m^{-1})^2 + \Delta\omega_M^2} + T_{2O}^{-1} \quad (2)$$

where T_{2O}^{-1} is the transverse relaxation rate of the nitrile in the outersphere, $\Delta\omega_M$ is the chemical shift difference between the coordinated and uncoordinated nitrile, τ_m^{-1} is the resident time of the nitrile ligand on the metal complex, and T_{2M}^{-1} is the transverse relaxation rate due to the coordinated nitrile which is determined by:

$$T_{2M}^{-1} = \frac{S(S+1)}{3}\left(\frac{2\pi A}{h}\right)^2\frac{1}{T_{1e}^{-1} + \tau_m^{-1}} \quad (3)$$

where S is the spin of the metal complex with the sixth ligand bound, $2\pi A/h$ is the hyperfine coupling constant between the unpaired electron and the α-carbon (which was assigned as 10 MHz over the temperature range investigated) and T_{1e}^{-1} is the electronic longitudinal relaxation rate. T_{1e}^{-1} was determined as previously described by Yamamoto et al.[19] over the temperature range investigated. The temperature dependence of $\Delta\omega_M^2$ is given by:

$$\Delta\omega_M = \omega_1\frac{g_e\mu_B}{\gamma_1}\left(\frac{2\pi A}{h}\right)\frac{S(S+1)}{3k_BT} \quad (4)$$

where ω_1 is the resonance frequency of the carbon nucleus, g_e is the *g*-value for a free electron, μ_B is the Bohr magneton, γ_1 is the gyromagnetic ratio for carbon, k_B is the Boltzmann's constant, and T is temperature. The exchange rate (k_{ex}) was then determined by:

$$\tau_m^{-1} = k_{ex} \quad (5)$$

(13) Schweitzer, D.; Shearer, J.; Rittenberg, D. K.; Shoner, S. C.; Ellison, J. J.; Loloee, R.; Lovell, S.; Barnhart, D.; Kovacs, J. A. *Inorg. Chem.* **2002**, *41*, 3128−3136.
(14) Shearer, J.; Nehring, J.; Lovell, S.; Kaminsky, W.; Kovacs, J. A. *Inorg. Chem.* **2001**, *40*, 5483−5484.
(15) Grant, D. H. *J. Chem. Educ.* **1995**, *72*, 39−40.
(16) *Igor Pro*, 3.15; Wavemetrics, Inc.: Lake Oswego, OR, 2000.
(17) Van Geet, A. L. *Anal. Chem.* **1968**, *40*, 2227−2229.
(18) *NUTS*; Acorn NMR, Inc.: Livermore, CA, 1997.
(19) Yamamoto, Y.; Nanai, N.; Chûjô, R. *Bull. Chem. Soc. Jpn.* **1991**, *64*, 3199−3201.

4-*tert*-Butylpyridine was used to determine pyridine exchange rates from **1** and **2**. In this case there is negligible unpaired spin density on the *tert*-butyl group carbons so that the exchange rate can be determined by:

$$T_{2P}P_M^{-1} = \pi(\Delta\nu_{cplx} - \Delta\nu_{solv})P_M^{-1} - T_{2O} = k_{ex} \quad (6)$$

The parameters $\Delta H^{\ddagger}$ and $\Delta S^{\ddagger}$ and E_a were then determined through standard procedures.[20]

XAS Sample Preparation and Data Collection. Complex **2** was dissolved in either CH_2Cl_2, MeCN, or MeOH (5−25 mg in ∼300 μL), injected into an aluminum sample holder between two pieces of translucent electrical tape (3M, no. 1205, Minneapolis, MN), and quickly frozen in liquid nitrogen. Data were collected at the National Synchrotron Light Source (Brookhaven National Laboratories, Upton, NY) on beamline X-9B using a focused Si(111) double-crystal monochromator, a low-angle nickel mirror for harmonic rejection, and a 13-element Ge solid-state fluorescence detector (Canberra). A helium Displex cryostat was used to keep the samples at a constant 77 K throughout the data collection. X-ray energies were calibrated by simultaneous measurement of the absorption spectrum of Fe foil (first inflection point assigned to 7111.2 eV).[21] The spectra were measured in 5 eV increments in the preedge region (6960−7100 eV), 0.5 and 1.5 eV increments in the edge region (7100−7132 and 7132−7171 eV), and 3 eV increments in the EXAFS region (7171−7910 eV).

XAS Data Analysis. The XAS baseline was normalized using a three-region cubic-spline function. The EXAFS region of the XAS was plotted against the wavevector *k*:

$$k = \pi[8m_e(E - E_o)]^{1/2}/h \quad (7)$$

where $E_o = 7125$ eV. Simulations used the single-scatterer (SS) EXAFS equation:

$$\chi_{calc} = \sum_{i=1}^{\#shells} n_i f_i k_i^{-1} r_i^{-2} \exp(-2\sigma_i^2 k_i^2) \sin(2k_i r_i + \alpha_i) \quad (8)$$

where n_i is the number of scatterers in the *i*th shell, r_i is their average distance from the metal center, σ_i is the variability (disorder) in that shell, and k_i is defined as:

$$k_i = \pi[8m_e(E - (7125\text{ eV} + \Delta E_i))]^{1/2}/h \quad (9)$$

where ΔE_i is the difference in energy between the nominal edge and the true ionization energy of that shell. This parameter fixed at $\Delta E_i = -0.5$ eV based on previous studies of similar complexes with known structures.[22] The amplitude and phase functions, generated by FEFF 7.01[23] simulations, were the same as we used previously.[22] We determined the baseline and edge height from simulations of the entire XAS (including Gaussian simulations of preedge peaks and first-coordination sphere fits to the EXAFS region) and then performed subsequent fits only on the EXAFS region to investigate alternative coordination models and the effects of including outer sphere scatterers. For fits that we report in this paper, we used weighted Fourier-filtered fits of $k^3\chi$ (FT: 1.0−14.3 Å; BT: $r' = 0.8-2.0$ Å).[33a] We also performed (but do not report) fits to unfiltered $k^2\chi$ in which the outer-sphere atoms were modeled as Fe−C shells at ca. 2.9, 3.4, and 4 Å; only the distances from the first of these shells corresponded to distances seen in crystal structures, while the longer distances probably were artifacts due to modeling multiple-scattering EXAFS using single-scattering theory. Our interest was primarily in the Fe-ligand bond lengths and disorder, and these parameters were virtually the same in the Fourier-filtered and -unfiltered fits. The least-squares error index ϵ^2 is defined as:

$$\epsilon^2 = [n_{idp}(n_{idp} - n_p)] \times \text{average}\{[(y_{data} - y_{calc})/\sigma_{data}]\}^2 \quad (10)$$

where n_{idp} is the number of independent[25] points in the data (y_{data} = Fourier-filtered $k^3\chi$), n_p is the number of refined parameters, and σ_{data} is the uncertainty attributed to the (Fourier-filtered) XAS spectrum, which is linearly interpolated from (k·Å, σ_{data}·Å^3) = (2.2, 0.19), (4.0, 0.26), (8.0, 0.26), (10.0, 0.42), (13.0, 0.88), (14.3, 0.56).[33a] Using criteria established by the International Workshops on Standards and Criteria in XAFS,[25] any model that gives shell-specific ϵ_s^2 values within 1 of the minimum achieved value should be considered a model consistent with the EXAFS data, although models with lower ϵ_s^2 values may be considered more likely. The reported parameter uncertainties were determined in the recommended manner by fixing the parameter in question at a series of values and refining all other parameters (that were refined in the original fit) to determine the variation that causes an increase in ϵ^2 by 1. The allowed variation range was generally slightly asymmetric; the larger of the allowed positive or negative variation from the best-fit value is reported as the ± value.

Bond valence sums analysis (BVS) of the EXAFS data was performed according to eq 11:

$$\text{BVS} = \sum s_{ij} \quad (11)$$

where s_{ij} is the valence of an individual bond described by:

$$s_{ij} = \exp[(R_o - R_{ij})/0.37] \quad (12)$$

where R_o is the length of a valence unit and R_{ij} is the experimentally determined bond length. The values used for R_o are: 1.759 Å for Fe−O, 1.831 Å for Fe−N, and 2.151 Å for Fe−S.[33a]

X-ray Crystallography of 2-NCS. X-ray-quality crystals were grown by slowly diffusing diethyl ether into a THF solution of **2-NCS** at −35 °C. A suitable single crystal was immersed in Paratone 8277 oil, mounted on a glass capillary, and immediately placed under a stream of cold dinitrogen gas. X-ray data was collected at 130 K using a Nonius Kappa CCD diffractometer. The structure was solved using direct methods and refined using SHELEX 97.[26] All hydrogen atoms were placed in an idealized geometry and refined using a riding model. Crystallographic data for **2-NCS** are listed in Table 1.

Results and Discussion

Reactivity of Five-Coordinate [Fe(III)($S_2^{Me2}N_3$(Pr,Pr))]$^+$ (1) and [Fe(III)($S_2^{Me2}N_3$(Et,Pr))]$^+$ (2) toward a Sixth Ligand. Recent calculations by Richards and co-workers indicate that the metal−amide bond in NHase has significant double-bond character between the nitrogen and carbon, and is best represented as an imido−metal bond (Scheme 2).[27] This is supported by modeling studies done in our group which show that the spectroscopic and electronic properties of NHase can be nicely reproduced with six-coordinate metal complexes containing imine nitrogens and *cis*-thiolates.[28] [Fe(III)($S_2^{Me2}N_3$(Pr,Pr))]$^+$

(20) Moore, J. W.; Pearson, R. G. *Kinetics and Mechanism: A Study of Homogeneous Chemical Reactions*, 3rd ed; John Wiley & Sons: New York, 1981; Chapter 5.
(21) Bearden, J. A.; Burr, A. F. *CRC Handbook, 60th ed.*; Weast, R. C., Astle, M. J., Eds.; CRC Press: Boca Raton, Fl. 1979. p E-193.
(22) Scarrow, R. C.; Stickler, B. S.; Ellison, J. J.; Shoner, S. C.; Kovacs, J. A.; Cummings, J. C.; Nelson, M. J. *J. Am. Chem. Soc*. **1998**, *120*, 9237−9245.
(23) Ankudinov, A. L.; Rehr, J. J. Phys. Rev. **1997**, B56, R1712−R1715.
(24) Ankudinov, A. L.; Ravel, B.; Rehr, J. J.; Conradson, S. D. *Phys. Rev. B.* **1998**, *58*, 7565−7576.
(25) Bunker, G., Hasnain, S., Sayers, D. In *X-ray Absorption Fine Structure*; Hasnain, S. S., Ed.; Ellis Horwood: New York, 1991; pp 751−770.
(26) (a) Otinowski, Z.; Minor, W. *Methods Enzymol.* **1996**, *276*, 307−326. (b) Blessing, R. H. *Acta Crystallogr. Sect. A* **1995**, *51*, 33. (c) Altomare, A.; Cascarano, G.; Giacovazzo, C.; Burla, M. C.; Polidori, G.; Camalli, M. *J. Appl. Crystallogr*. **1994**, *27*, 435−442. (d) Sheldrick, G. M. *SHELEX97* University of Gottingen.
(27) Boone, A. J.; Cory, M. G.; Scott, M. J.; Zerner, M. C.; Richards, N. G. J. *Inorg. Chem.* **2001**, *40*, 1837−1845.

Table 1. Crystallographic Data for [Fe(III)$S_2^{Me2}N_3$(Et,Pr)(SCN)] (**2-NCS**)

	2-NCS
formula	$C_{16}H_{29}FeN_4S_3$
molecular mass	429.48
crystal color, habit	plate, dark-red
T (K)	130(2)
crystal system	orthorhombic
space group	*Pbca* (No. 61)
a (Å)	10.8846(5)
b (Å)	15.6740(5)
c (Å)	23.5810(10)
α (deg)	90
β (deg)	90
γ (deg)	90
V (Å^3)	4023.0(3)
Z	8
ρ_{calcd} (g cm^{-3})	1.418
μ(Mo Kα) (mm^{-1})	1.067
Θ range (deg)	2−26
collected reflections	7342
unique reflections	3938
number of parameters	227
GOF[a] on F^2	0.885
R1[b] (wR2[c]) (%)	3.94 (7.85)

[a] GOF = $\{\sum[w(F_o^2 - F_c^2)^2]/(M - N)\}^{1/2}$ (M = number of reflections, N = number of parameters refined). [b] R1 = $\sum||F_o| - |F_c||/\sum|F_o|$ for $I > 2\sigma(I)$. [c] wR2 = $\{\sum[w(F_o^2 - F_c^2)^2]/\sum[w(F_o^2)^2]\}^{1/2}$ using all data.

Scheme 2. Metal Amide Resonance Form Showing Relation to Metal Imine

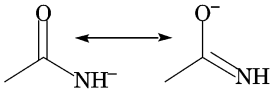

amidate **imidate**

(**1**) was previously shown to reversibly bind azide; however, it appeared to be unreactive toward neutral ligands such as MeCN and alcohols, on the basis of ambient temperature electronic absorption studies.[10] Reexamination of the low-temperature EPR spectrum of **1** in a *noncoordinating solvent* mixture (CH_2Cl_2/toluene glass) indicated that this may not necessarily be the case. When the EPR spectrum of **1** is recorded in a rigorously dried CH_2Cl_2/toluene (1:1) glass (Figure S-19), a distorted pseudo-rhombic EPR spectrum is observed ($g = 2.15, 2.07, 2.00$), which differs from that of **1** in a MeOH/EtOH glass (2.20, 2.15, 2.00). In the noncoordinating solvent, a less rhombic signal, with a narrower *g*-spread, is observed. Addition of MeOH or EtOH to this CH_2Cl_2/toluene solution converted the $g = 2.15, 2.07, 2.00$ signal to a more rhombic signal (2.20, 2.15, 2.00), identical to that of **1** in MeOH/EtOH. This suggested that alcohols bind to the metal center of **1** at 150 K. In this manner, it was determined that in CH_2Cl_2/toluene solution, a wide variety of neutral ligands (including nitriles), as well as SCN^-, bind to **1** at extremely low temperatures (≤150 K).

Recently,[13] we showed that the removal of a methylene unit from the ligand backbone of **1** to afford [Fe(III)($S_2^{Me2}N_3$-(Et,Pr))]$^+$ (**2**), results in a more distorted structure (Figure 2, $\tau = 0.52$ (**2**) vs $\tau = 0.76$ (**1**)).[29] This subtle distortion in structure altered the magnetic properties and increased the reactivity of **2** relative to that of **1**.[13] It was determined that **2** reacts faster with azide than **1** and that azide dissociates an order of magnitude slower from the resulting complex **2-N$_3$** versus **1-N$_3$**. It was therefore not surprising that **2** was also found to bind a wider variety of ligands at higher temperatures relative to **1**. Ligand binding was screened using EPR (Table 2), in a CH_2Cl_2/toluene glass at 150 K. As was seen with **1**, the distorted pseudo-rhombic EPR spectrum of **2** converts to the more rhombic spectrum of six-coordinate **2-L** upon the addition of Lewis bases (L) in noncoordinating solvents. This is illustrated in Figure 3 for L = MeCN.

Table 2. Ligand Binding to [Fe(III)($S_2^{Me2}N_3$(Et,Pr))]$^+$ (**2**) Monitored by Low-Temperature UV/Vis Spectroscopy and EPR

2-L	EPR[a]	low-*T* electronic spectrum, λ_{max}[b]
2	2.12, 2.07, 2.02	−
2-MeCN	2.17, 2.14, 2.01	830 nm
2-EtCN	2.17, 2.13, 2.01	830 nm
2-^{t}BuCN	2.16, 2.13, 2.01	813 nm
2-PhCN	2.17, 2.13, 2.01	845 nm
2-py	2.17, 2.15, 2.00	765 nm
2-N_3^-	2.18, 2.15, 1.98	760 nm
2-SCN^-	2.18, 2.16, 2.00	[c]806 nm
2-^{t}BuNC	2.15, 2.10, 2.01	[c]877 nm
2-MeOH	2.18, 2.15, 2.00	753 nm
2-EtOH	2.17, 2.14, 2.02	742 nm
2-$CH_3C(O)NH_2$	2.18, 2.16, 2.00	*d*
2-$CH_3C(O)CH_3$	2.16, 2.12, 2.00	745 nm
2-$CH_3SC(NH)CH_3$	2.16, 2.00	*d*

[a] X-Band at 150 K; CH_2Cl_2/toluene. [b] In CH_2Cl_2 solution at −90 °C. Only the low-energy band (above 700 nm) is reported. [c] Binds at room temperature in CH_2Cl_2. [d] Insoluble at temperatures below −20 °C.

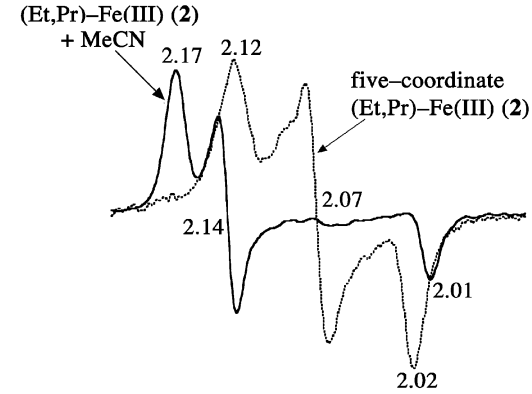

Figure 3. X-band EPR spectrum of [Fe(III)($S_2^{Me2}N_3$(Et,Pr))]PF_6 (**2**) in CH_2Cl_2/toluene (1:1) glass, both in the absence and presence of MeCN.

EPR screening of reactivity was performed in frozen glasses at 150 K, whereas enzymes function at considerably higher temperatures, and in solution. To examine the reactivity of **1** and **2** under more relevant conditions, reactivity was screened in solutions of methylene chloride over the temperature range −90−0 °C. This is where the major differences in reactivity between **1** and **2** become apparent. For both complexes, as a sixth ligand binds to the metal, a low-energy charge-transfer band centered near 800 nm grows in (Figure 4). A similar charge-transfer band is also observed in the active form of Fe−NHase.[5,6] Under these conditions (methylene chloride, −90 °C), **1** does not appear to bind any nitriles or alcohols, and the only amine it will bind under these conditions is pyridine. With anionic ligands such as azide or thiocyanate, on the other hand, only 1 equiv of ligand is required to observe complete binding to **1** (and **2**) at −90 °C in CH_2Cl_2.

(28) (a) Shoner, S. C.; Barnhart, D.; Kovacs, J. A. *Inorg. Chem.* **1995**, *34*, 4517−4518. (b) Jackson, H. L.; Shoner, S. C.; Rittenberg, D.; Cowen, J. A.; Lovell, S.; Barnhart D.; Kovacs, J. A. *Inorg. Chem.* **2001**, *40*, 1646−1653.

(29) τ is defined as (α−*β*)/60, where α = largest angle, *β* = second largest angle ($\tau = 1.0$ for ideal trigonal bipyramidal; $\tau = 0.0$ for ideal square pyramidal). Addison, A. W.; Rao, T. N.; Reedijk, J.; Van Rijn, J.; Verschoor, G. C. *J. Chem. Soc., Dalton Trans.* **1984**, 1349−1356.

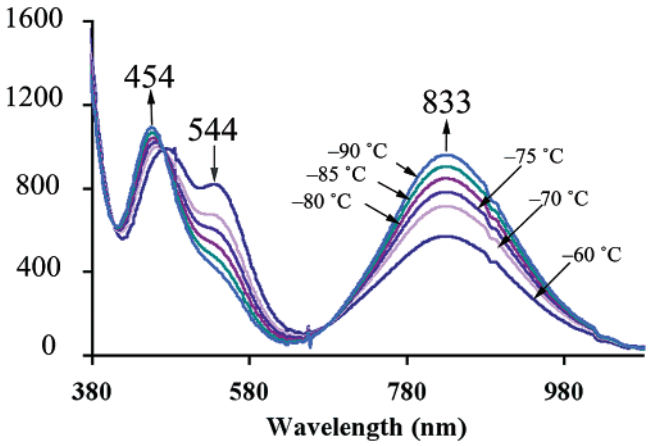

Figure 4. Temperature-dependent electronic absorption spectrum of [Fe(III)($S_2^{Me2}N_3$(Et,Pr))]PF_6 (**2**) + MeCN (5000 equiv) in CH_2Cl_2. As the temperature is lowered, two bands corresponding to [Fe(III)($S_2^{Me2}N_3$-(Et,Pr))(MeCN)]PF_6 (**2-MeCN**) appear at 454 and 833 nm, and a shoulder at 544 nm, corresponding to **2**, disappears. The ratio of MeCN bound to five-coordinate **2** changes from 55% at −60 °C, to 69% at −70 °C, 77% at −75 °C, 83% at −80 °C, 90% at −85 °C, and 100% at −90 °C.

In contrast to **1**, **2** binds a wide variety of "substrates" including nitriles (benzonitrile, acetonitrile, *iso*-propionitrile) and alcohols (methanol, ethanol, propanol), as well as pyridine, acetamide, acetone, and thiocyanate in methylene chloride solutions at −90 °C (Table 2). Nitrile binding is reversible, and an excess of nitrile is required to observe complete binding. For example, in a methylene chloride solution of **2**, 5000 equiv of MeCN are required to observe complete binding at −90 °C. As the temperature is increased, the concentration of five-coordinate **2** increases relative to that of six-coordinate **2-MeCN** (Figure 4). When **2** is dissolved in neat MeCN, 12% of MeCN-bound **2-MeCN** is detected at ambient temperature. In contrast, <1% of MeCN-bound **1-MeCN** is detected in neat MeCN, even at temperatures as low as −46 °C. This illustrates how dramatically the affinity for nitriles increases upon removal of a methylene unit from (Pr,Pr)-ligated **1** and is yet another indication of the inherent increase in reactivity of **2** compared with that of **1**.

(Et,Pr)-ligated **2** has a much lower affinity for alcohols relative to nitriles. Complete binding of methanol to **2** is not observed even in neat methanol just above its freezing point (−98 °C). In methanolic solutions, nitriles preferentially bind to **2**, even when there is a large excess of MeOH present. Competitive binding studies show that the equilibrium constant for **2-MeOH** formation is an order of magnitude smaller than K_{eq} for **2-MeCN** formation. When **2** is dissolved in a solvent consisting of an 11:1 MeOH/MeCN mixture, a broad absorption band (width at half-height = 205 nm) is observed, which is red-shifted (789 nm) almost halfway between the λ_{max} for **2-MeOH** (753 nm) and λ_{max} for **2-MeCN** (830 nm). This indicates that roughly a 1:1 ratio of **2-MeCN**:**2-MeOH** forms when an 11-fold excess of MeOH is present, indicating that K_{eq}(**2-MeCN**) is roughly an order of magnitude larger than K_{eq}(**2-MeOH**). Given that water is a poorer Lewis base than MeOH, this result implies that $K_{eq}(H_2O)$ would be *more* than an order of magnitude smaller than K_{eq}(MeCN). Proposed mechanism 3 would require that a nitrile displace water in the first step of nitrile hydrolysis by NHase. Our results suggest that *a nitrile would be capable of displacing water from the active-site* of NHase. However, this would require that the hydroxide, shown (by ENDOR) to be coordinated to the iron site,[30] be protonated prior to substrate binding. NHase activity has been shown to decrease[5e,31] as the pH is raised above pH = 7.3 consistent with this possibility. Mascharak recently reported that the pK_a of water bound to Fe(III) in a ligand environment similar to **2** is around 6.8.[9] Furthermore, he reports an extremely large $-\Delta H$ value for water binding to this compound. When the results described herein are taken into account, it is conceivable that Mascharak is dealing with a hydroxide-bound, as opposed to water-bound species. However, it is also conceivable that the amide ligands make his system sufficiently electron-rich to raise the pK_a of his Fe(III)−OH to the point where the protonated form is favored. With **2**, hydroxide attacks the carbon of the imine bond in the ligand backbone, rather than the metal, and water does not compete adequately enough with the coordinating solvents required to solubilize **2** (acetone, MeCN, DMF) to generate significant quantities of water-bound **2-H_2O**, even at low temperatures. The spectrum of **2** in a MeCN/H_2O (75:25) is identical to that of **2** in MeCN. In noncoordinating solvents, such as CH_2Cl_2, the concentration of water is too low to favor the six-coordinate, water-bound form.

Synthesis and Structure of [Fe^{III}($S_2^{Me2}N_3$(Et,Pr))] (2-NCS). As was observed with **1**, anionic ligand binding is more favored than neutral ligand binding to **2** in methylene chloride, or acetonitrile. Only 1 equiv of N_3^- or SCN^-, for example, is required to observe complete binding to **2** at −90 °C. This encouraged us to prepare a thiocyanate-bound derivative of **2** (**2-NCS**). Having a structurally characterized thiocyanate complex would aid in the analysis of EXAFS data for nitrile-bound **2-MeCN** (vide infra), by providing an example of a linearly coordinated ligand that might be involved in multiple scattering.

Thiocyanate-ligated **2-NCS** was synthesized by adding 2 equiv of thiocyanate to a MeCN solution of **2** at ambient temperature. The ν_{SCN} stretch at 2058 cm^{-1} (vs 2107 cm^{-1} for free thiocyanate) in the IR demonstrated that SCN^- was coordinated to the metal. Single crystals (red plates) of **2-SCN** were grown from THF/diethyl ether. The solution-state magnetic moment (2.31 μ_B (in MeCN) and EPR parameters (g = 2.183, 2.164, 2.004) indicate that **2-SCN** is low-spin ($S = {}^1/_2$) at both ambient temperature and 150 K, respectively. In CH_2Cl_2, **2-NCS** displays a LMCT band at 833(1020) nm in its electronic absorption spectrum. This band is not observed with the five-coordinate parent compound **2**. If crystalline **2-NCS** is dissolved in methanol at ambient temperature, this LMCT band disappears, and the spectrum reverts back to that associated with five-coordinate **2**, indicating that thiocyanate binds reversibly under these conditions. To unambiguously confirm the structure of **2-NCS** an X-ray crystal structure was determined.

The X-ray crystal structure shows that the Fe center of **2-NCS** is contained in a distorted octahedral coordination environment with a nearly linear N-bound thiocyanate (Fe−N(4)−C(16) = 178.5°) coordinated trans to a thiolate (Figure 5). Substrates bind in a similar fashion, that is, trans to a cysteinate sulfur, in NHase. The C=N bond length of the bound thiocyanate (1.172(4) Å) is slightly longer than that of free thiocyanate

(30) Doan, P. E.; Nelson, M. J.; Jin, H.; Hoffman, B. M. *J. Am. Chem. Soc.* **1996**, *118*, 7014−7015.
(31) Cramp, R. A.; Cowan, D. A. *Biochim. Biophys. Acta* **1999**, *1431*, 249−260.

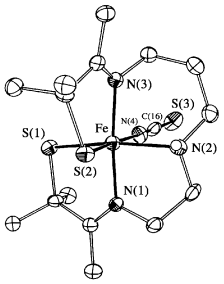

Figure 5. ORTEP diagram of thiocyanate-bound [Fe(III)($S_2^{Me2}N_3$(Et,Pr)-(NCS)] (**2-NCS**), showing 50% probability ellipsoids and atom-labeling scheme. All H atoms, except for the N(2)−H proton, have been omitted for clarity.

(1.15 Å). The average Fe−S bond length (2.214(9) Å) in **2-NCS** is ∼0.1 Å longer than that of **2** (2.117(1)). This increase in bond length is the expected result of increasing the coordination number and is similar to that observed upon coordination of azide to **1**[10] and **2**.[13] The average Fe−S bond length in these model compounds compares well with the average EXAFS-determined Fe−S distance (2.20 Å) in the active form of Fe−NHase. The average Fe−N bond lengths (1.986 (3) Å) in **2-NCS** also compare well with the EXAFS-determined average Fe−N bond lengths found in Fe−NHase (1.99 Å).

Fe K-Edge X-ray Absorption Spectroscopy (XAS) of 2, [$Fe^{III}(S_2^{Me2}N_3$(Et,Pr))(MeCN)](PF_6) (2-MeCN), and [$Fe^{III}(S_2^{Me2}N_3$(Et,Pr))(MeOH)](PF_6) (2-MeOH). Compounds **2-MeCN** and **2-MeOH** would not yield isolable solids; therefore, XAS was used to determine the structures of solvent-bound **2**. The X-ray absorption spectra of **2** were recorded in frozen solutions of methylene chloride, acetonitrile, and methanol. The preedge region of the spectra of **2** in all three solutions is dominated by an absorbance at 7112 eV that is attributed to a 1s → 3d transition (Figure 6). Upon dissolution of **2** in the coordinating solvents acetonitrile and methanol, the area under this peak decreases by a factor of 2 when compared to that when **2** is dissolved in the noncoordinating solvent methylene chloride. Que and co-workers have previously demonstrated that the size of this transition is an indication of the degree of symmetry about the metal center.[32] In complexes with centrosymmetric metal environments, such as square planar or octahedral, the area of the 1s → 3d transition is less than that of the area for noncentrosymmetric five-coordinate environments. The results from analysis of the preedge indicates that the Fe(III) center of **2** dissolved in acetonitrile and methanol is more centrosymmetric than that of **2** dissolved in methylene chloride, consistent with the addition of a sixth ligand from solvent in acetonitrile and methanol, but not in the methylene chloride solution.

Fourier transforms and simulations of the EXAFS for all three compounds (Figure 7) show that contributions from the first coordination sphere dominate the EXAFS. The parameters from the fits shown in Figure 7 are given in Table 3. The coordination model assumed complete chelation by the $S_2^{Me2}N_3$(Et,Pr) ligand and the presence of a sixth oxygen or nitrogen from solvent **2-MeOH** or **2-MeCN**, respectively, based on the XANES analysis presented above. The calculated bond lengths of 2.00(2) Å (Fe−N) and 2.12(2) Å (Fe−S) for five-coordinate **2** in CH_2Cl_2

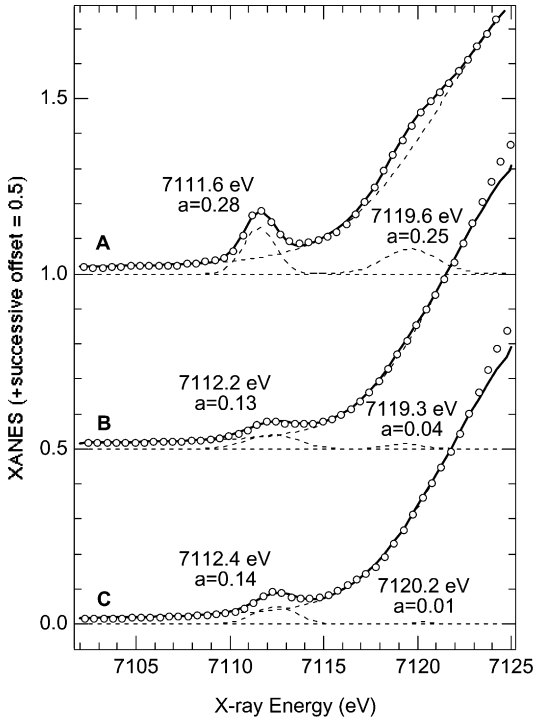

Figure 6. 1s → 3d transition found in the XAS of **2** (a), **2**-MeOH (b), and **2**-MeCN (c). Relative heights for all spectra are identical. Data are depicted as circles (ooo), fit of data is depicted as the solid line (−), and the deconvolution of the preedge into an edge shape and two Gaussian peaks is depicted as the dashed line (- - -) The refined peak positions and areas (in units of eV × fractional edge height) are indicated.

solution compare with the average bond lengths previously determined for crystalline five-coordinate **1** (1.99 and 2.15 Å)[10a] and **2** (1.95 and 2.12 Å).[13] The biggest discrepancy between the solution and crystal structure distances is the average Fe−N bond length, which is 0.05 Å shorter in the crystal structure. This difference may be due to distortions caused by crystal packing or even possibly due to systematic errors in the Fe−N bond lengths caused by the symmetry-imposed disorder of the Et and Pr ligand backbones within the structure of **2**.[13]

Bond valence sum analysis (BVS) has previously proven useful in interpreting the EXAFS results for metal complexes.[33] Here the EXAFS determined bond lengths for the different scatterers are compared with a reference metal−ligand distance to estimate the valence of each bond. These are then summed, giving a BVS. For a metal complex in given oxidation- and spin states, the BVS for the complex should center around a given value. If a ligand is added to the metal complex, the average bond lengths about the metal center should increase; however, the BVS should not dramatically change if there is no change in spin- or oxidation state. Thus, BVS can provide good estimates of the oxidation- and spin states of a metal complex if only the bond lengths are known. If the oxidation- and spin states for the complex are already known, then BVS can provide an internal check to determine if the number and

(32) (a) Randall, C. R.; Shu, L.; Chiou, Y.-M.; Kagen, K. S.; Ito, M.; Kitajima, N.; Lachicotte, R. J.; Zang, Y.; Que, L., Jr. *Inorg. Chem.* **1985**, *34*, 1036−1039. (b) Roe, A. L.; Schneider, D. J.; Mayer, R. J.; Pyrz, J. W.; Widom, J.; Que, L., Jr. *J. Am. Chem. Soc.* **1984**, *106*, 1676−1681.

(33) (a) Scarrow, R. C.; Brennan, B. A.; Cummings, J. G.; Jin, H.; Duong, D. J.; Kindt, J. T.; Nelson, M. J. *Biochemistry* **1996**, *35*, 10078−10088. (b) Brown, I. D.; Altermatt, D. *Acta Crystallogr., Sect. B* **1985**, *41*, 244−247. (c) Thorp, H. H. *Inorg. Chem.* **1998**, *37*, 5690−5692. (d) Garner, C. D. *Physica B* **1995**, *209*, 714−716. (e) Hati, S.; Datta, D. *J. Chem. Soc., Dalton Trans.* **1995**, 1177−1182. (f) Thorp, H. H. *Inorg. Chem.* **1992**, *31*, 1585. (g) Liu, W.; Thorp, H. H. *Inorg. Chem.* **1993**, *32*, 4102−4105. (h) Palenik, G. J. *Inorg. Chem.* **1997**, *36*, 4888−4890. (i) Palenik, G. J. *Inorg. Chem.* **1997**, *36*, 3394−3397. (j) Palenik, G. J. *Inorg. Chem.* **1997**, *36*, 122.

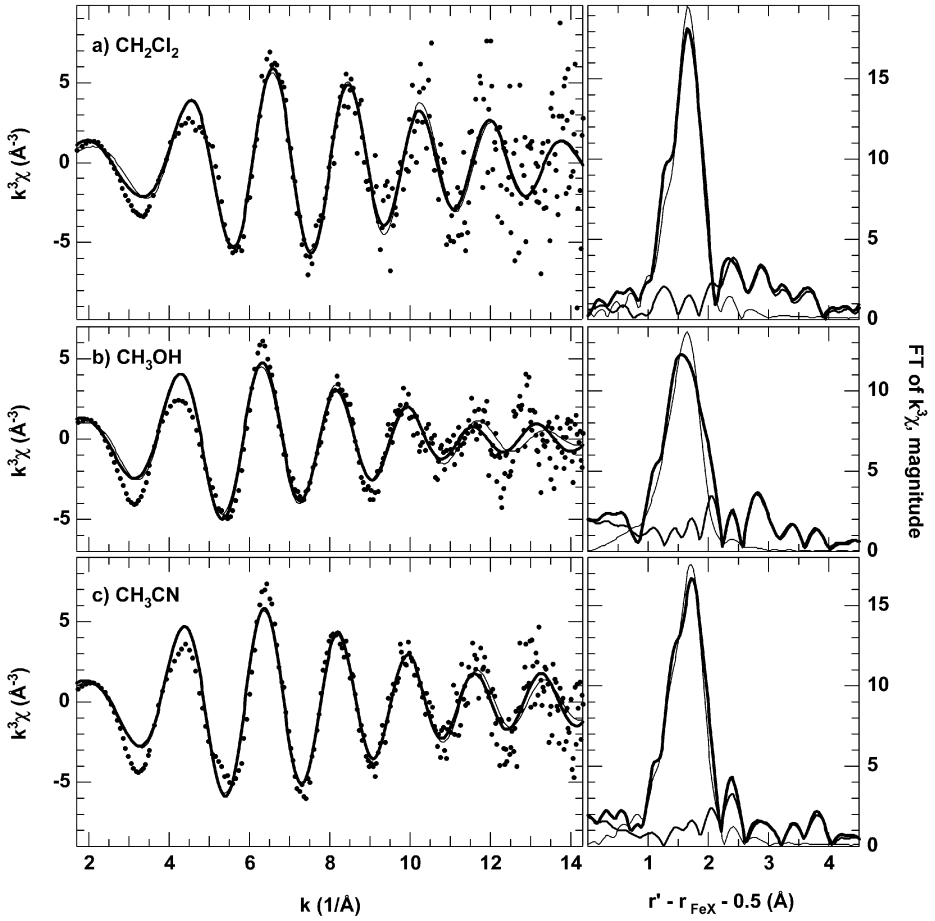

Figure 7. Unfiltered k^3 EXAFS (left, circles), FT over $k = 1.0$ to 14.3 Å^{-1} (right) and first sphere FF using backtransform limits of $r' = 0.8-2.0$ Å (left). For FT and FF spectra, the thick line is the data, and the thin line shows the fit using parameters from Table 3; the FT magnitude of the difference spectrum is shown by a line of medium thickness. Data are shown for **2** in CH_2Cl_2 (a), **2-MeOH** (b), and **2-MeCN** (c).

Table 3. EXAFS Data Refinements for **2**, **2-MeOH**, and **2-MeCN**

	2 (in CH_2Cl_2)	**2-MeOH**	**2-MeCN**
N_{N+O}	3 N[a]	3 N + 1 O[b]	4 N
r_{N+O} (Å)	2.000 ± 0.018[c]	2.033 ± 0.016	2.017 ± 0.016
σ_{N+O} (Å)[d]	0.075 ± 0.030	0.093 ± 0.025	0.108 ± 0.019
N_S	2 S	2 S	2 S
r_S (Å)	2.117 ± 0.015	2.179 ± 0.021	2.179 ± 0.010
σ_S (Å)	0.070 ± 0.019	0.093 ± 0.025	0.067 ± 0.012
BVS	4.09 ± 0.13[e]	4.07 ± 0.14	4.28 ± 0.09
ϵ^2	2.2	2.0	0.7

[a] The number of N and S scatterers was held fixed at the values shown. [b] For **2**-MeOH, an oxygen scatterer was included with its r and σ constrained to be the same as for the nitrogen shell. [c] Uncertainty range is for ϵ^2 no more than 1.0 greater than the minimum value reported. [d] σ^2, the Debye−Waller disorder parameter, was refined. The best-fit values and uncertainty ranges were converted to σ values because the uncertainty ranges were more symmetrical when expressed in σ rather than σ^2. [e] Uncertainty range determined by mapping ϵ^2 in a series of refinments in which BVS was fixed to a value (4.00, for instance) and r_{N+O} and the two σ parameters were refined, while r_S was constrained to be consistent with the fixed BVS.

distance of the different scatterers are correct. When the bond lengths determined for **2** (Table 3) are analyzed by this method, the BVS is 4.1 ± 0.1. For comparison, the crystal structure bond lengths of **1** and **2** give BVS values of 4.0 and 4.4, respectively. All three of these values fall within the range of 3.7−4.5 previously determined for low-spin Fe^{3+} complexes (average value = 4.1).[33a] Thus, the existence of a low-spin ferric center in **2** is supported by the BVS analysis as well as by both magnetic and EPR data.

The Fe−N and Fe−S distances determined by EXAFS analysis lengthen by 0.02−0.06 Å in the six-coordinate **2-MeOH** and **2-MeCN** compared with those in five-coordinate **2**. Similar bond distance increases are observed upon comparison of the crystal structures of the azide adducts and the corresponding five-coordinate **1** and **2**.[10,13] The lengthening of bonds is required in order to keep the BVS within the range expected upon addition of a sixth ligand.

As noted above, the number of N and S scatterers in the refinements of Table 3 were fixed at values expected on the basis of the coordination numbers suggested by XANES. In all three cases, the quality of fit improves (ϵ^2 is decreased) when the number of nitrogen scatterers in the model is increased by one (i.e., from 3 to 4, or from 4 to 5). This would suggest six-coordination for **2** in CH_2Cl_2 and seven-coordination for **2-MeOH** and **2-MeCN**. Despite the better fit to the data, these simulations yield unprecedentedly high BVS (4.6 to 4.8) and also high refined disorder factors ($\sigma_N > 0.10$ Å) for the Fe−N shell. The seven-coordinate models for the methanol and acetonitrile adducts seem particularly unlikely. Thus, we discount the suggestion of higher coordination numbers from the EXAFS fitting and attribute the better fits to slight inaccuracies in the amplitude and phase functions, an inac-

curately determined E_0, or incomplete removal of outer sphere EXAFS contributions by the Fourier filtering.

It was previously demonstrated that multiple scattering (MS) pathways were important in fitting the EXAFS of an Fe−NHase model containing NO because of the nearly linear Fe−N−O bond angle (172°). We therefore expected MS pathways to be crucial in fitting the EXAFS data for **2-MeCN**, because of the expected near linear iron−nitrile bond. To test this expectation, we used FEFF 7.02[23] to simulate single- and multiple-scattering EXAFS for a structure based on the coordinates of **2-N_3**, but with the azide replaced by a linear $NCCH_3$ ligand. From these simulations we isolated contributions to the EXAFS due only to the Fe−$NCCH_3$ unit. Results of these simulations are shown in the Supporting Information (Figure S-20). When only a linear Fe−$NCCH_3$ unit was considered, peaks in the $k^3\chi$ FT EXAFS spectrum occurred at $r' = 2.8$ and 4.2 Å, and these peaks were about 3 times larger than the magnitude of the $k^3\chi$ FT EXAFS for **2-MeCN** at the same values of r'. However, as the Fe−N−C angle was varied from 180° to 164° (a variation found in acetonitrile complexes in the Cambridge Structure Database),[34] the magnitude of the $r' = 4.2$ Å peak was cut in half. Furthermore, when the coordinates of the $S_2{}^{Me2}N_3$(Pr,Pr) ligand were added into the simulation, scattering from the C atoms of the ligand caused destructive interference with the $r' = 2.8$ Å peak due to the acetonitrile ligand, so that $r' = 2.8$ Å became a minimum in the FT magnitude. Finally, when the FEFF 7.02 program was asked to simulate vibrational disorder, the magnitude in both the first coordination sphere ($r' = 1-2$ Å) and outer sphere ($r' > 2$ Å) regions of the FT EXAFS were reduced so that the magnitudes in the simulations were similar to those of the data of **2-MeCN**. Thus, our expectation of observing multiple-scattering effects from a single acetonitrile ligand was not realized, and may not be possible due to competing single- and multiple-scattering pathways due to the ligand $S_2{}^{Me2}N_3$(Et,Pr).

Thermodynamics of Ligand Binding. Neutral ligands were found to bind reversibly to **1** and **2** and induce dramatic changes to the electronic absorption spectra. Thus, thermodynamic parameters for ligand binding could easily be obtained spectrophotometrically. Equilibrium constants (K_{eq}) for reactions converting **1** or **2** to **1-L** or **2-L** were determined (Tables S-8−S-11) at several different temperatures according to standard procedures.[10,13,35−36] Van't Hoff plots (Figures S-8−S-11) were then used to extract the enthalpy and entropy parameters for the reaction.

Thermodynamic parameters for the binding of neutral ligands to **1** and **2** were determined as previously described for azide, except methylene chloride was used in place of MeOH. This was done to ensure that the added ligand would not have to compete with a coordinating solvent. Analysis of the temperature dependence of K_{eq}'s for MeCN binding to **2** using a van't Hoff plot showed that MeCN binds with an enthalpy similar to that of azide ($\Delta H = -7.5 \pm 0.6$ kcal/mol). The entropy for nitrile binding to **2** ($\Delta S = -30 \pm 6$ eu) was determined, however, to be substantially more negative than for azide binding ($\Delta S = -16.6 \pm 2.5$ eu). Solvation effects could account for these differences. Azide anions are very effectively solvated by methanol, whereas MeCN is not effectively solvated by methylene chloride. Thus, azide is in an inherently more ordered state in methanol than is MeCN in methylene chloride, contributing to a smaller than expected ΔS.

To determine if there is any selectivity in nitrile binding to **2**, we examined the reactivity of **2** with a variety of nitriles under the conditions necessary to measure thermodynamic parameters. Unfortunately, nitriles such as *iso*-propionitrile and *tert*-butyl nitrile were found to precipitate out of solution before complete binding was observed at −90 °C. Aside from acetonitrile, the only nitrile that did not precipitate under these conditions was benzonitrile. The ΔH for benzonitrile binding to **2** was determined to be −4.2(±0.8) kcal/mol. This smaller enthalpy change relative to MeCN can be rationalized from two different perspectives. First, the electron-withdrawing properties of the phenyl ring results in an inherently less Lewis basic nitrile with PhCN when compared with MeCN. This would result in a weaker Fe−N bond if the nitrile were mainly acting as a σ-donor, as opposed to a π-acceptor. Second, given that the Ph group is substantially larger than a methyl group, it is likely that steric interactions between PhCN and the ligand backbone of **2** would also weaken the Fe−NC bond relative to MeCN. The ΔS associated with benzonitrile binding to **2** was determined to be −18(±4) eu. This is substantially lower than the entropy change associated with MeCN binding. Such a result can be rationalized if, prior to its coordination to the metal, the PhCN molecules were involved in, for example, some type of π-stacking interaction. This would create a more ordered unbound state relative to MeCN.

To compare the affinities of (Et,Pr)-ligated **2** versus that of (Pr,Pr)-ligated **1** for neutral ligands, we needed to identify a ligand which would bind to *both* **1** and **2** at temperatures above the freezing point of CH_2Cl_2. The only ligand that fit this criterion was pyridine. Pyridine binding to **1** requires a large excess of ligand, and the reaction is highly reversible. Complete binding is only observed when >5000 equiv of pyridine are added to a methylene chloride solution of **1** at −90 °C. As the temperature is increased, the electronic absorption peaks due to five-coordinate **1** grow at the expense of those due to **1-py**. Above −20 °C there is no evidence of pyridine-bound **1-py** in the spectrum. Pyridine binding to **2** is also reversible, and 6500 equiv of pyridine are required to observe complete binding at −90 °C. The thermodynamic parameters for pyridine binding to **1** and **2** (ΔH(**1-py**) = −6.3(1) kcal/mol, ΔS(**1-py**) = −29.0(3) eu, ΔH(**2-py**) = −8.2(6) kcal/mol, ΔS(**2-py**) = −41(3) eu) were determined spectrophotometrically and are compared in Tables S-10 and S-11. In contrast to what one might expect, at any given temperature the equilibrium constant for py binding to **2** is smaller than that of MeCN binding. Most likely the greater steric bulk of the phenyl ring is responsible for the unusually low affinity of **2** for pyridine. This would be consistent with the PhCN results. The smaller barrier to ligand exchange with the bulkier PhCN and py ligands is also consistent with this explanation (vide infra).

Kinetics of Ligand Exchange. Dynamic NMR analysis was used to determined the rates of nitrile ligand exchange from **2** and the rates of pyridine exchange from both **1** and **2**.[37] Nitriles were not observed to bind to **1** at temperatures accessible in

(34) Allen, F. H.; Davies, J. E.; Galloy, J. J.; Johnson, O.; Kennard, O.; Macrae, C. F.; Mitchell, E. M.; Mitchell, G. F.; Smith, J. M.; Watson, D. G. *J. Chem. Inf. Comput. Sci.* **1991**, *31*, 187−204.
(35) Guidry, R. M.; Drago, R. S. *J. Am. Chem. Soc.* **1973**, *95*, 6645.
(36) Epley, T. D.; Drago, R. S. *J. Am. Chem. Soc.* **1969**, *91*, 2883.

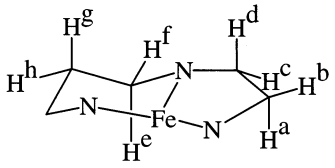

Figure 8. Atom-labeling scheme of the (Et,Pr) backbone in **2**.

Table 4. Proton Chemical Shift Assignments of the Et,Pr Backbone of **2** as Derived through Proton Longitudinal Relaxation Rates at 303 K (500 MHz)

atom label	chemical shift (ppm)	distance from Fe (Å)[a]	distance from Fe (Å)[b]	T_1 (msec)
H^a	22.92	3.01	2.79	2.338
H^b	−10.61	3.54	3.42	6.266
H^c	19.78	3.19	3.19	3.324
H^d	26.51	3.14	3.09	3.053
H^e	−22.05	3.12	3.08	2.875
H^f	5.65	3.22	3.15	3.480
H^g	−9.72	3.89	3.97	9.917
H^h	5.32	4.10	4.18	15.243
H^i	−11.40	3.82	3.72	10.900
H^j	−31.81	3.09	2.85	2.741

[a] Calculated from T_1 values. [b] Calculated from crystal structure.

the NMR experiment. It was previously shown that eq 2 (see Experimental Section) could be used to determine the rate of nitrile exchange with bulk solvent for a series of Mn^{2+} complexes.[38] Thus, it was reasoned that this equation could be applied to our system.

The electronic transverse relaxation rate (T_{1e}^{-1}) was determined as previously described.[19] Briefly, by measuring transverse relaxation rates for protons (T_1^{-1}) in the backbone of **2** and plotting this as a function of r^{-6} (Figure S-1) one can extract the T_{1e}^{-1} value from the slope using the following equation:

$$T_1^{-1} = (2/5)S(S+1)\gamma_H^2 g_H^2 \beta^2 T_{1e} r^{-6} \qquad (13)$$

Proton chemical shift assignments (Figure 8) and proton−iron distances were determined via T_1 relaxation times, and NOE difference spectroscopy (Table 4, Figure S-2). The resulting distances were consistent with those expected on the basis of the X-ray crystal structure of **2**.[13] Using this analysis for **2**, T_{1e}^{-1} was determined to obey the following relationship as a function of temperature:

$$T_{1e}^{-1} = [2.33 \times 10^{-1} \exp(0.008147T)]10^{11}\ \mathrm{sec}^{-1} \quad (14)$$

over the temperature range of 190−313 K (Figure S-1). This value falls within the expected T_{1e}^{-1} value for a low-spin Fe(III) complex.[39]

The rates for nitrile exchange (k_{ex}) from **2-RCN** were calculated using eqs (1−5) (see Experimental Section). Using this analysis, it was determined that k_{ex} for MeCN exchange from **2-MeCN** varies significantly with temperature. As the temperature is lowered to near the freezing point of a CH_2Cl_2/MeCN mixture, the exchange rate decreases from 2.51(1) × 10^5 sec^{-1} at 300 K to 1.71(3) × 10^2 sec^{-1} at ∼180 K (Table S-1). When this analysis is applied to **1**, no observable line-broadening is observed in the ^{13}C NMR (over the temperature range of 190−300 K) that can be attributed to chemical exchange, indicating that MeCN does not bind to **1** over this temperature range.

Table 5. Activation Parameters and 275 K k_{ex} for 2-RCN, **2-py$^{4-t\mathrm{Bu}}$**, and **1-py$^{4-t\mathrm{Bu}}$**

	k_{ex}^{275} (sec^{-1})	$\Delta H^{\ddagger}$ (kcal/mol)	$\Delta S^{\ddagger}$ (eu)	E_a (kcal/mol)
2-MeCN	8.50(2) × 10^4	7.1(8)	−10(1)	7.3(8)
2-PhCN	3.27(2) × 10^4	4.9(8)	−20(3)	5.3(9)
2-^{i}PrCN	3.27(2) × 10^4	5.4(6)	−17(2)	6.0(7)
2-py$^{4-t\mathrm{Bu}}$	3.56(3) × 10^4	5(1)	−18(2)	6(1)
1-py$^{4-t\mathrm{Bu}}$	1.19(3) × 10^5	3.1(8)	−25.8(3)	3.7(9)

The ambient temperature exchange rate, k_{ex}, for MeCN (Table 5) is considerably faster than one would expect for a low-spin Fe(III) complex. For example, the low-spin thiolate-ligated Fe(III) complex $[Fe(III)(S^{Me2}N_5(tren)(MeCN))]^{2+}$ (**3**) (Figure 10) also undergoes nitrile exchange at room temperature with bulk solvent; however, the rate of MeCN exchange from **3** (k_{ex} = 1.25(1) × 10^1 sec^{-1} at 293 K) is nearly *4 orders of magnitude slower than that found for **2-MeCN***.[40] This decrease in rate could be explained on the basis of differences in molecular charge (+2 with **3** vs +1 with **2-MeCN**); however, it is unlikely that charge differences could account for such disparity in rates. Previously, we demonstrated that the *trans*-thiolate of the low-spin Co(III) complex $[Co(III)(S_2^{Me2}N_3(Pr,Pr)]^+$ increases anionic ligand dissociation rates by 4 orders of magnitude relative to $[Co(III)(NH_3)_5(H_2O)]^{3+}$.[41] Complex **3** lacks a thiolate trans to the MeCN binding site, whereas **2-MeCN** contains this structural feature. Thus one might *conclude that the trans thiolate aids the displacement of the nitrile from the metal center of **2-MeCN***. NHase also possesses a cysteinate trans to its substrate-binding site, which might assist product displacement from the NHase metal center. This would explain how low-spin metal centers can be utilized as catalysts in metalloenzymes involved in substrate binding and product release. As shown here and elsewhere,[41] a *trans*-cysteinate is capable of turning a relatively inert metal center into a labile metal center.

To determine how electronic effects influence nitrile exchange rates from **2-RCN**, we compared MeCN exchange rates with those of benzonitrile (PhCN). Exchange rates, k_{ex}, for PhCN are comparable to those of MeCN (Table S-2). Activation parameters differ significantly, however (Table 5). As illustrated in the Eyring plot of Figure 9 and in Table 5, $\Delta H^{\ddagger}$ for MeCN exchange is roughly 2.3 kcal/mol higher than for PhCN exchange.

This smaller barrier to exchange for PhCN could be a consequence of the electron-withdrawing properties of the phenyl group which decrease the Lewis basicity of the nitrile, thus weakening the Fe−N bond. Another possibility is that unfavorable steric interactions between the bulkier phenyl group and the ligand backbone of **2** favor the displacement of PhCN from **2-NCPh**. To determine how sterics might influence nitrile exchange rates from **2-RCN**, the rates of *iso*-propionitrile (^{i}PrCN) exchange were measured (Table S-3) and compared

(37) (a) Kaplan, J. I.; Fraenkel, G. *NMR of Chemically Exchanging Systems*; Academic Press Inc.: New York, 1980. (b) Sandström, J. *Dynamic NMR Spectroscopy*; Academic Press Inc.: New York, 1982.
(38) Inada, Y.; Sugata, T.; Ozutsumi, K.; Shigenobu, F. *Inorg. Chem.* **1998**, *37*, 1886−1891.
(39) Walker, F. A. *Spectroscopic Methods in Bioinorganic Chemistry*; Solomon, E. I., Hodgson, K. O., Eds; ACS Symposium Series 692; American Chemical Society: Washington, DC, 1998; p 37.
(40) Shearer, J. *Models For Metalloenzymes Containing Sulfur-Metal Bonds*. Doctoral Thesis, University of Washington, Seattle, WA, 2001.
(41) Shearer, J.; Kung, I. Y.; Lovell, S.; Kaminsky, W.; Kovacs, J. A. *J. Am. Chem. Soc.* **2001**, *123*, 463−468.

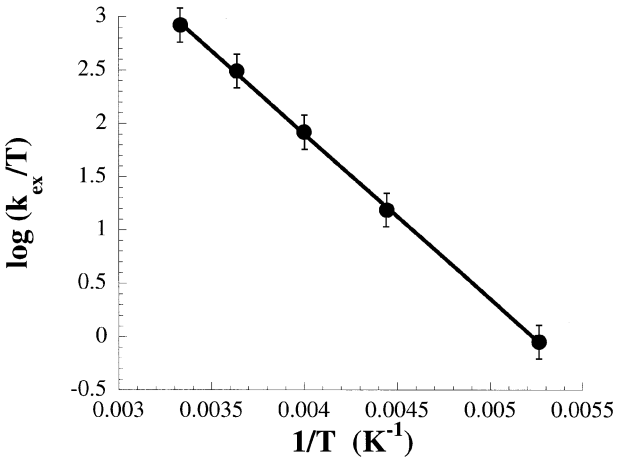

Figure 9. Eyring plot for the exchange of MeCN from **2-MeCN**.

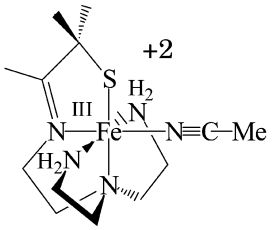

Figure 10. Structure of $[Fe(III)(S^{Me2}N_5(tren)(MeCN)]^{2+}$ (**3**).[14]

with those of MeCN and PhCN. The *A* value for a Ph group is larger than the *A* value for an ^{i}Pr group ($A_{Ph} = 3.0$ kcal/mol vs $A_{iPr} = 2.21$ kcal/mol),[42] suggesting that if sterics *do* play a role in nitrile exchange, one would expect $\Delta H^{\ddagger}$(^{i}PrCN) to be smaller than $\Delta H^{\ddagger}$(MeCN), but larger than $\Delta H^{\ddagger}$(PhCN). However, if sterics do *not* play a significant role, then $\Delta H^{\ddagger}$(^{i}PrCN) should be approximately the same as $\Delta H^{\ddagger}$(MeCN). As was found with PhCN, the ambient temperature k_{ex} rates for **2-^{i}PrCN** are comparable to those of **2-MeCN**, while the $\Delta H^{\ddagger}$ for ^{i}PrCN exchange from **2-^{i}PrCN** is significantly lower than that of **2-MeCN** (Table 5). This suggests that steric factors *do* play a role in promoting the displacement of both ^{i}PrCN and PhCN from **2-RCN** when compared to MeCN. As was determined with MeCN, ^{i}PrCN and PhCN do not appear to bind to **1** under the conditions used to determine k_{ex} rates.

The rates of azide binding to **1** and **2** were previously compared.[13] It was determined that azide binds ~3 times faster to **2** relative to **1**. This was attributed to the more distorted, less stable geometry and more accessible metal ion of **2** relative to that of **1**. Furthermore, azide was found to dissociate from **2-N$_3$** ~1 order of magnitude slower than from **1-N$_3$**. This was attributed to the more strained geometry of **1-N$_3$** compared to that of **2-N$_3$**. To obtain further evidence for this structural difference having an influence on reaction kinetics, we attempted to determine the k_{ex} for the exchange of neutral ligands from both **1** and **2**. Unfortunately **1** was shown to be unreactive toward nitriles and alcohols under the conditions examined. However, both **1** and **2** readily bind pyridine.

(42) *A* is defined as the difference in energy between a functional group being in the axial vs equatorial position of a cyclohexane ring, and is a measure of steric bulk. (a) Booth, H.; Everett, J. R. *J. Chem. Soc., Chem. Commun.* **1976**, 278. (b) Booth, H.; Everett, J. R. *J. Chem. Soc., Perkin Trans. 2* **1980**, 255. (c) Hirsch, J. A. *Top. Stereochem.* **1967**, *1*, 199.

Variable-temperature pyridine binding kinetics were performed using 4-*tert*-butyl pyridine (4-^{t}BuPy) as the substrate. The *tert*-butyl derivative of pyridine provides a nice spectroscopic handle, because there is negligible unpaired spin-density located on the *tert*-butyl group. As a result, there should be no observable line broadening of these NMR peaks due to Fermi contact interaction. Thus, all of the line broadening should be directly related to dynamic and outer-sphere relaxation processes. Hence, eq 6 (see Experimental Section) can be used directly to determine ^{t}BuPy exchange kinetics. To further eliminate error in the calculation of k_{ex} the tertiary carbon on the *tert*-butyl group was monitored, as opposed to the methyl group carbons. This eliminated contributions due to other dynamic processes, such as rotation of the methyl groups, that may be affected by temperature.

The k_{ex} for 4-^{t}BuPy exchange from **1** was measured over the temperature range of 190−300 K (Table S-5), and was determined to vary from 6.56×10^3 to 2.31×10^5 s^{-1}, which is comparable to nitrile exchange from **2**. The activation parameters for 4-^{t}BuPy exchange from **1** *do* noticeably differ, however, from the activation parameters for nitrile exchange from **2** (Table 5). For example, $\Delta H^{\ddagger}$ for 4-^{t}BuPy exchange from **1** (3.1(8) kcal/mol) is considerably lower than $\Delta H^{\ddagger}$ for MeCN exchange from **2** (7.1(8) kcal/mol). Rates for 4-^{t}BuPy exchange from **2** were determined over the temperature range 225−300 K (Table S-4). With this compound, considerably slower exchange rates at temperatures below 200 K prevented determination of exchange rates for 4-^{t}BuPy exchange from **2** at lower temperatures. Rates varied from 1.74×10^3 to 5.79×10^4 s^{-1}, which is about *an order of magnitude slower than* those observed for **1**. This translates into a $\Delta H^{\ddagger}$ for 4-^{t}BuPy exchange from **2-py^{4-tBu}** of 5(1) kcal/mol, which is 1.9 kcal/mol higher than $\Delta H^{\ddagger}$ (**1-py^{4-tBu}**). This finding is consistent with the higher barrier to azide exchange from **2-N$_3$** versus **1-N$_3$** and appears to suggest that the transition-state enthalpies for **1** and **2** are similar, with the difference in reaction enthalpies being derived from the relative stabilities of the products. The $\Delta H^{\ddagger}$ for 4-^{t}BuPy exchange from **2-py^{4-tBu}** is comparable with that of PhCN exchange from **2-PhCN**, and both are considerably smaller than that of MeCN exchange from **2-MeCN** (Table 5). This provides additional evidence to suggest that steric repulsions are in part responsible for the rapid exchange of ligands which introduce bulk directed toward the metal of the complexes described herein.

Summary and Conclusions

This work demonstrates for the first time that nitriles can reversibly bind to iron when it is in a ligand environment resembling that of NHase. The resulting nitrile-bound complex displays spectroscopic (electronic-absorption, EPR) and structural (spin-state, average Fe−S and Fe−N bond lengths) properties similar to that of Fe−NHase. Such work lends validity to the proposed mechanism in which nitrile C≡N bond activation occurs via a coordinated Fe−NCR intermediate. Also, we have demonstrated that ligand exchange in a system resembling that of NHase is rapid, showing that a low-spin first-row transition metal can be a competent catalyst in an enzyme reaction that involves substrate displacement from the metal center. Faster than expected ligand exchange rates with these systems are attributed to the labilizing effects of a *trans*-thiolate. When this structural feature is removed and replaced with a

trans nitrogen, rapid ligand exchange is no longer observed. NHase also possesses a thiolate trans to the substrate-binding site. It thus appears that nature utilizes the labilizing effect of a *trans*-thiolate to improve product off-rates from the metal center of NHase.

Acknowledgment. We thank Steven Schultz and Vincent Pons for experimental assistance with the collection of low-temperature NMR spectra. This work was supported by the NIH (Grant No. GM 45881). Research carried out (in part) at the National Synchrotron Light Source, Brookhaven National Laboratory, was supported by the U.S. Department of Energy, Division of Materials Sciences and Division of Chemical Sciences.

Supporting Information Available: Variable-temperature NMR kinetics results for **2-MeCN**, **2-^{i}PrCN**, **2-PhCN**, **1-py**, **2-py** (Tables S-1−S-5), temperature dependence of T_{1e}^{-1} for **2** (Figure S-1), the ^{1}H NMR spectrum of **2** (Figures S-2), equilibrium constants (Tables S-6−S-9), van't Hoff plots (Figures S-8−S-11) for ligand binding to **1** and **2**, variable-temperature electronic absorption spectra (Figures S-3−S-7), and EPR spectra for "substrate"-bound **2** (Figures S-12−S-19), and crystallographic data for 2-NCS (Tables S-10−S-14) (PDF). This material is available free of charge via the Internet at http://pubs.acs.org.

JA012555F